Modeling Heterogeneous $ClNO_2$ Formation, Chloride Availability, and Chlorine Cycling in Southeast Texas

Simon, H.[a,*], Y. Kimura[b], G. McGaughey[b], D. T. Allen[b], S. S. Brown[c], D. Coffman[d], J. Dibb[e], H.D. Osthoff[f], P. Quinn[d], J.M. Roberts[c], G. Yarwood[g], S. Kemball-Cook,[g] D. Byun[h], and D. Lee[h]

[a]Center for Energy and Environmental Resources, University of Texas at Austin, 10100 Burnet Road, Bldg. 133, R7100, Austin, Texas 78758 and National Exposure Research Laboratory, U.S. Environmental Protection Agency, 109 T.W. Alexander Dr., Research Triangle Park, NC, 27711
[b]Center for Energy and Environmental Resources, University of Texas at Austin, 10100 Burnet Road, Bldg. 133, R7100, Austin, Texas 78758
[c]NOAA/ESRL Chemical Sciences Division, 325 Broadway, Boulder, CO 80305, USA
[d]NOAA/OAR Pacific Marine Environmental Laboratory, 7600 Sand Point Way NE Seattle, WA 98115
[e]University of New Hampshire, Climate Change Research Center, Morse Hall Rm 361, Durham, NH 03824
[f]NOAA/ESRL Chemical Sciences Division, 325 Broadway, Boulder, CO 80305, USA present address: University of Calgary, Department of Chemistry, 2500 University Drive NW, Calgary, AB T2N 1N4, Canada
[g]Environ International Corp, 773 San Marin Drive, Suite 2115, Novato, CA 94998
[h]Department of Earth and Atmospheric Sciences, University of Houston, 312 Science & Research 1, Rm #312, Houston, TX 77204-5007
[*]corresponding author. Tel: +1-919-541-1803; fax +1-919-541-1379. E-mail address: Simon.Heather@epa.gov

Abstract

Nitryl Chloride ($ClNO_2$) mixing ratios above 1 ppbv have been measured off the coast of Southeast Texas. $ClNO_2$ formation, the result of heterogeneous N_2O_5 uptake on chloride-containing aerosols, has a significant impact on oxidant formation for the Houston area. This work reports on the modeling of $ClNO_2$ formation and describes the sensitivity of $ClNO_2$ formation to key parameters. Model sensitivity analyses found that: (1) Chloride availability limits the formation of nitryl chloride at ground level but not aloft; (2) When excess particulate chloride was assumed to be present at ground level through sea salt, $ClNO_2$ concentrations increased in some locations by a factor of 13, as compared to cases where sea salt chloride was assumed to be limited; (3) Inland formation of $ClNO_2$ seems feasible based on chloride availability and could have a large impact on total $ClNO_2$ formed in the region; and (4) $ClNO_2$ formation is quite sensitive to the assumed yield of $ClNO_2$ from N_2O_5 uptake. These results demonstrate that there is a need for further field studies to better understand the geographic extent of $ClNO_2$ formation and the atmospheric conditions which control partitioning of chloride into the particle phase. In addition, this work examined the role of $ClNO_2$ in the cycling of chlorine between chloride and reactive chlorine radicals. The modeling indicated that the majority of reactive chlorine in Texas along the Gulf coast is cycled through $ClNO_2$, demonstrating the importance of including $ClNO_2$ into photochemical models for this region.

Key Words: Nitryl Chloride, chlorine, CAMx, urban air pollution, Houston, GoMACCS, TexAQS II, heterogeneous chemistry

1. Introduction

Ambient measurements of Nitryl Chloride ($ClNO_2$) were made for the first time during the TexAQS II/GoMACCS field campaign in 2006 (Osthoff et al., 2008).

$ClNO_2$ mixing ratios measured on board the *Research Vessel Ronald H Brown* reached over 1 part per billion by volume (ppbv) off the coast of southeast Texas. This compound is potentially significant for several reasons. First, $ClNO_2$ serves as a NO_x reservoir at night which prevents nitrogen from being lost to inactive forms such as nitric acid. Second, $ClNO_2$ represents a largely unstudied form of chlorine in the atmosphere that may be a key step in a pathway that converts particulate chloride into reactive chlorine radicals. The effect of this chemistry on both NO_x and chlorine cycling has the potential to increase ozone production in regionally polluted areas (Simon et al., 2009; Osthoff et al., 2008).

Finlayson-Pitts et al (1989) first suggested that $ClNO_2$ could form from heterogeneous reactions between N_2O_5 and aqueous sea salt aerosols. Osthoff et al (2008) showed strong temporal correlations between $ClNO_2$ and N_2O_5 concentrations measured in the Gulf of Mexico. Their results make a compelling case that the dominant mechanism for nitryl chloride formation is this heterogeneous pathway. Studies that have investigated heterogeneous $ClNO_2$ formation in the laboratory suggest that the mechanism is the same as that of heterogeneous N_2O_5 hydrolysis [Reaction (1)] (Behnke et al., 1997; Schweitzer et al., 1998).

$$N_2O_5 \xrightarrow{aqueous\ \ sea\ \ salt} NO_2^+ + NO_3^- \qquad \text{Reaction (1)}$$

The Cl^- ions in aqueous aerosol compete with H_2O to react with NO_2^+. Therefore the reaction can either result in $2HNO_3$ or $ClNO_2 + HNO_3$ as shown in Reactions (2), (3), and (4).

$$NO_3^-(aq) + H^+(aq) \rightarrow HNO_3(g) \qquad \text{Reaction (2)}$$

$$NO_2^+(aq) + Cl^-(aq) \rightarrow ClNO_2(g) \qquad \text{Reaction (3)}$$

$$NO_2^+(aq) + 2H_2O(aq) \rightarrow HNO_3(g) + H_3O^+(aq) \qquad \text{Reaction (4)}$$

97 The yield of nitryl chloride from this reaction [i.e. the fraction of NO_2^+ ions that
98 proceed to Reaction (3) instead of Reaction (4)] is strongly dependent on the chloride
99 ion concentration in the aerosol (Behnke et al., 1997; Roberts et al., 2009; Schweitzer
100 et al., 1998; Thornton and Abbott, 2005; Roberts et al., 2009). Yields close to 1 at
101 high molarities (1M) suggest that Cl^- ions outcompete H_2O as discussed in section
102 3.2.3. In fact, both Behnke et al. (1997) and Roberts et al. (2009) report nitryl
103 chloride formation on aerosols as dilute as 0.01M. Most laboratory studies are in
104 relative agreement on their measurements of reactive uptake coefficients for N_2O_5 on
105 chloride aerosols (0.01-0.03) (Behnke et al., 1997; Schweitzer et al., 1998; Thornton
106 and Abbott, 2005).

107 Previous articles have described the impact of $ClNO_2$, once formed, on ozone
108 formation (Simon et al., 2009; Osthoff et al., 2008). The work presented here
109 incorporated heterogeneous $ClNO_2$ formation on ambient aerosol, as well as other
110 related heterogeneous N_2O_5 chemistry, and investigated the sensitivity of $ClNO_2$
111 formation to various model parameters. Specifically, this work studies the
112 dependence of $ClNO_2$ formation on available chloride and its sensitivity to the
113 assumed yield of $ClNO_2$. Finally, the implications of this chemistry for chlorine
114 cycling and the total reactive chlorine budget in Southeast Texas are investigated.

115 **2. Methods**

116 **2.1 Photochemical Simulations**

117 Photochemical modeling was performed using the Comprehensive Air quality
118 Model with extensions (CAMx) version 4.2 (Environ, 2008). This program is a three-
119 dimensional Eulerian model which calculates the effects of emissions, chemistry,
120 deposition, advection, and dispersion on chemical concentrations in the atmosphere.
121 A full description of the model treatment of these processes as well as the nesting

schemes and numerical solvers can be found in the CAMx User's Guide (Environ, 2008). Evaluations of CAMx model performance have been carried out by Tesche et al. (2006) and Morris et al (2005). CAMx was chosen for this work to facilitate comparison with previous studies of chlorine and nitryl chloride in the Houston area (Chang and Allen, 2006a; Chang and Allen, 2006b; Wang et al., 2007; Simon et al., 2009).

The modeling domain consisted of three two-way nested grids, as shown in Figure 1. The two largest of these grids had cells with horizontal dimensions of 36 km by 36 km and 12 km by 12 km. These two grids have 17 vertical layers covering the lowest 15 km of the atmosphere. The finest of the grids, which was centered over the Houston area, had cells with horizontal dimensions of 4 km by 4 km and 28 vertical layers covering the lowest 15 km of the atmosphere. The layers are more finely divided at lower altitudes, with 12 of the 28 layers in the lowest 1000m. A full description of the thickness of each vertical layer is described by the Texas Commission on Environmental Quality for their SIP mid-course review modeling (http://www.tceq.state.tx.us/implementation/air/airmod/data/hgb1_camx_domain.html). The model simulation was run for the dates of August 30, 2006 through September 9, 2006, one of the time periods when the *R.V. Ronald H. Brown* was taking measurements in the Houston area. August 28 and 29 were used as model spin-up days. Meteorological inputs for the modeled days were developed at the University of Houston (Ngan, 2008), as described by Simon et al. (2009) and in the supplemental information.

Emissions inputs for ozone precursor compounds (NO_x and VOCs) are described by Simon, et al. (2009). In addition, emissions of anthropogenic Cl_2, primary particulate matter (PM), SO_2, and ammonia were included in the modeling.

147 A full description of these emissions and the associated boundary conditions can be
148 found in the supplemental information.

149 **2.2 Updated model chemistry**

150 Current versions of the CAMx software include a standard CB IV chemical
151 mechanism (Gery et al, 1989), and two enhanced mechanisms: one with added
152 chlorine chemistry described in Tanaka et al. (2003) and one with added aerosol
153 chemistry based on work by Pandis et al. (1993), Nenes et al. (1998), and Yarwood et
154 al. (2005). The aerosols in this model are categorized into 16 main species (sulfate,
155 nitrate, ammonium, water, 9 secondary organic aerosol species, sodium, chloride,
156 primary organic matter, elemental carbon, and 4 non-reactive species) and 4 size bins
157 (0.039 - 0.156 μm; 0.156 - 0.625 μm; 0.625 - 2.5 μm; and 2.5 - 10 μm). Since this
158 study entails modeling processes that interact both with chlorine and with aerosols,
159 the chlorine and aerosol chemistry were linked in a single mechanism.

160 To correctly model the heterogeneous conversion of N_2O_5 to $ClNO_2$, there are
161 several key factors that must be properly accounted for: the formation of NO_3 from O_3
162 + NO_2, the strongly temperature-dependant reversible inter-conversion of NO_3 and
163 N_2O_5, and the relative magnitudes of NO_3 and N_2O_5 losses. The formation and
164 destruction reactions of NO_3 are handled in CAMx's standard CB IV chemical
165 mechanism. The reactions of N_2O_5 are also, for the most part, included in the
166 standard chemical mechanism. A major uncertainty in the N_2O_5 chemistry in CAMx
167 is the loss mechanisms for N_2O_5 (both homogeneous and heterogeneous). Field
168 measurements suggest that gas-phase reactions of N_2O_5 are not a significant loss
169 pathway in the lower troposphere in southeast Texas (Brown et al., 2006; Brown et
170 al., 2009; Simon, 2008), so gas-phase hydrolysis of N_2O_5 was not included in the

171 model simulations. Changes to the heterogeneous chemistry used in this modeling are
172 discussed below.

173 The heterogeneous loss rate for N_2O_5 was calculated using Equation (1) and
174 the heterogeneous formation rate of $ClNO_2$ was calculated using Equation (2),

175 $$\frac{-d[N_2O_5]}{dt} = k[N_2O_5] = \frac{\gamma\omega A}{4}[N_2O_5] \qquad \text{Equation (1)}$$

176 $$\frac{d[ClNO_2]}{dt} = Yk[N_2O_5] = \frac{Y\gamma\omega A}{4}[N_2O_5] \qquad \text{Equation (2)}$$

177 where k (s^{-1}) is the first order rate constant for the heterogeneous reaction, Y is the
178 yield of $ClNO_2$ for each molecule of N_2O_5 reacted, γ is the reactive uptake coefficient
179 (the probability that a molecule of N_2O_5 which impacts a particle will react), ω (m/s)
180 is the mean molecular speed of the N_2O_5, and A (m^2/m^3 of air) is the total aerosol
181 surface area. For each time step, the total aerosol surface area was calculated based
182 on model predictions of speciated aerosol mass in each grid cell. For this calculation,
183 particles were assumed to be spherical with species-specific densities given by Simon
184 (2008). The assumption of spherical particles is reasonable since previous studies in
185 Texas have shown aerosol to be predominantly in a deliquesced state (Santarpia et al.,
186 2004). Mean particle diameters were taken as the geometric mean for each of four
187 PM size bins used. It should be noted that Equations (1) and (2) represent the change
188 in N_2O_5 and $ClNO_2$ concentrations from this specific chemistry and not the full
189 differential equation with all source and loss terms.

190 The reactive uptake coefficient is a complex function of aerosol composition
191 and relative humidity (Davis et al, 2008; Evans and Jacob, 2005). A recent study of
192 N_2O_5 reactivity in Texas showed that parameterization of $\gamma(N_2O_5)$ based on laboratory
193 studies are systematically larger than direct determinations from aircraft
194 measurements taken over inland areas during night flights (Brown et al., 2009).

195 However, N_2O_5 and $ClNO_2$ data from ship based measurements in Galveston Bay and
196 other location along the Gulf Coast were consistent with relatively larger $\gamma(N_2O_5)$, in
197 the range of 0.02-0.03 (Osthoff et al., 2008). On the basis of these empirical
198 observations, geographic location was used as a surrogate for $\gamma(N_2O_5)$ in this study.
199 Heterogeneous chemistry was only included in the 4 and 12 km modeling domain,
200 since the focus of this modeling is to evaluate chemistry in Southeast Texas. Because
201 model parameters were based on local ambient measurements, the chosen modeling
202 setup may not be applicable to other areas of the country. The 4 and 12 km domains
203 were split into 3 regions (see Figure 2): region 1 covered all marine and coastline grid
204 cells, region 2 covered the Houston Ship Channel, and region 3 covered all other
205 terrestrial grid cells. Although region 2 is small in area it was treated as a distinct
206 region because it includes a large number of industrial sources with freshly emitted
207 plumes that are expected to have an aerosol with a different composition from aerosol
208 in the rest of Texas. Heterogeneous N_2O_5 uptake was modeled using Reactions (5),
209 (6), and (7) for regions 1, 2, and 3 respectively. It should be noted that water as a
210 reactant is implied in these reactions, but is not explicitly shown.

211 $$N_2O_5 + PM \xrightarrow{\gamma=0.03} 0.75(ClNO_2 + HNO_3) + 0.25(2HNO_3) - 0.75HCl$$ Reaction (5)

212 $$N_2O_5 + PM \xrightarrow{\gamma=0.01} 2HNO_3$$ Reaction (6)

213 $$N_2O_5 + PM \xrightarrow{\gamma=0.001} 2HNO_3$$ Reaction (7)

214 Aldener et al (2006) reported a reactive uptake of 0.03 from ambient measurements
215 taken in the marine boundary layer. In addition, Osthoff et al. (2008) modeled data
216 using a $\gamma(N_2O_5)$ value of 0.025 for the TexAQS 2006 episode. Based on these two
217 studies, the reactive uptake coefficient for Reaction (5) was set to 0.03. Reaction (5)
218 represents a 75% yield of $ClNO_2$ with respect to N_2O_5 uptake. Osthoff et al. (2008)
219 reported yields from measurements in the Gulf of Mexico of between 18% and 100%.

220 The 75% yield is an intermediate value; however, the sensitivity of the model to this
221 value is tested in this work. Reaction (5) was added as a loss mechanism for HCl,
222 since one chlorine atom is required to form each $ClNO_2$ molecule. Given that CAMx
223 calculates a rapid equilibrium between gas-phase HCl and particle-phase chloride,
224 removing the HCl from the gas phase is essentially equivalent to removing it from the
225 particle phase. Reaction (5) was shut off [and N_2O_5 chemistry switched to reaction
226 (7)] when HCl mixing ratios dropped below 0.5 parts-per trillion by volume (pptv) to
227 prevent creation of chlorine mass. This threshold was taken as 0.1% of a typical HCl
228 concentration for the Houston area (0.5 ppbv) as reported by Chang and Allen
229 (2006b) and is assumed to be a lower bound for the concentration of chloride required
230 to form $ClNO_2$. This will give an upper-bound on the amount of $ClNO_2$ formed since
231 the model uses a constant yield until HCl concentrations reach this threshold, while
232 actual yields decrease at lower particulate chloride concentrations. The uncertainties
233 due to this assumption and the assumption of a constant 75% yield are discussed in
234 more detail below.

235 The reactive uptake coefficients in Regions 2 and 3 were based on
236 measurements made by Brown et al. (2009) and Brown et al. (2006). The reactive
237 uptake coefficient for region 2, an area characterized by non-neutralized sulfate
238 aerosols, was set at the upper end of the ambient measured values (0.01). The
239 reactive uptake coefficient for region 3, whose aerosol is composed of neutralized
240 ammonium sulfate and secondary organic aerosol, was set at the lower end of the
241 measured range (0.001). It is assumed that over terrestrial grid cells, Cl availability is
242 low and a negligible amount of $ClNO_2$ will form in these locations. However, the
243 sensitivity of the model to this assumption is evaluated below.

The final change made to the chemical mechanism in CAMx was the addition of the photolysis of $ClNO_2$ to form NO_2 and Cl as described in Simon et al (2009).

Results

3.1 Model predictions of N_2O_5, $ClNO_2$, and HNO_3 mixing ratios

Maximum and average hourly ground-level mixing ratios of N_2O_5, $ClNO_2$, and HNO_3 in the 4km domain are shown in Table 1. The values were calculated for each night in the simulation for the hours of 10pm to 5am. Average values for $ClNO_2$ mixing ratios are reported only over marine grid cells where formation occurs in the model. Maximum predicted $ClNO_2$ mixing ratios ranged from 256 pptv to 1210 pptv on different nights. The maximum 1-minute average $ClNO_2$ mixing ratio measured aboard the *Research Vessel Ronald H Brown* during the TexAQS II/GoMACCS field study was just above 1300 pptv, similar to the maximum $ClNO_2$ concentrations in the model. More detailed comparisons between model predictions and ambient measurements for PM surface area, N_2O_5, HNO_3, and $ClNO_2$ mixing ratios are given in the supplemental information. These comparisons show that predicted values using this modeling scheme are generally consistent with measured values, except in the Houston Ship Channel, where $ClNO_2$ concentrations are consistent with measurements and N_2O_5 is over-predicted. Inaccuracies in this region are likely due to uncertainties in the emissions inventory or sub-grid cell phenomena associated with localized plumes.

Figure 3 shows the spatial distribution of the species on the night of Aug 30 – Aug 31, 2006. The spatial distribution of N_2O_5 depends on the location of NO_x in urban and industrial plumes. The major NO_x plumes on every night originated from Houston, TX, Beaumont, TX, and Lake Charles, LA. PM surface area was also highest in these three urban/industrial areas. The spatial distribution NO_3 and N_2O_5

mixing ratios were the same, which is expected since there is rapid inter-conversion between these two compounds in the model. HNO_3 and $ClNO_2$ follow the same spatial patterns as N_2O_5 except for the fact that $ClNO_2$ was mostly restricted to marine and near-marine grid cells. For the Houston area, it appears that the NO_x and aerosol surface area are highest in the source region, while N_2O_5, $ClNO_2$, and HNO_3 are highest downwind. This pattern is to be expected at night since NO_2 reacts with ozone to form NO_3 and eventually N_2O_5. Therefore the NO_2 is generally observed in fresh plumes and the N_2O_5 and its reaction products reach peak concentrations several hours downwind of the source region.

3.2 Evaluation of Chloride availability and its effect on $ClNO_2$ production

Even with data from measurements taken during TexAQS II, there is still a great deal of uncertainty about parameters used to model heterogeneous N_2O_5 chemistry. One key uncertainty is the availability of chloride. This can affect the $ClNO_2$ yield from heterogeneous N_2O_5 uptake and the geographic extent of these reactions. A set of sensitivity runs was performed to further evaluate the assumptions about chloride availability that were made in this model simulation.

3.2.1 Effect of using the HCl switch

The methods described above include techniques implemented to account for the depletion of HCl due to $ClNO_2$ formation and for the fact that heterogeneous uptake will not result in $ClNO_2$ formation unless there is particulate chloride present. The two elements of this technique were 1) the loss of an HCl molecule for every $ClNO_2$ molecule formed [see Reaction (5)] and 2) an "HCl switch" (based on the assumption that gas-phase and particulate chloride are rapidly exchanged). When the gas-phase HCl, and therefore total chloride, concentration dropped below a minimum level (0.5 pptv) all $ClNO_2$ formation was turned off. Further evaluation of the

sensitivity of the model to this "HCl switch" chemistry can give insight into how chloride limitation is affecting the heterogeneous N_2O_5 chemistry. Two sensitivity runs are used to evaluate this dependency further.

3.2.1.1 $ClNO_2$ Formation in the Presence of Excess Chloride

In this sensitivity run, $ClNO_2$ formation was modeled as if it were not dependent on chloride availability. To do this, the "HCl switch" was always on. There was no loss of HCl when $ClNO_2$ formed and $ClNO_2$ formation depended solely on location ($ClNO_2$ formation was still restricted to marine grid cells), surface area concentration, and N_2O_5 mixing ratio, and not on the predicted HCl mixing ratio. Results from this run indicate how much $ClNO_2$ would form if there were a surplus of chloride present in the atmosphere.

This run shows significant increases in HCl mixing ratios in areas where $ClNO_2$ is present. Figure 4 shows the predicted HCl mixing ratios on September 1, 2006 at 5am in the base case simulation and the predicted increases in HCl caused by eliminating HCl loss due to $ClNO_2$ formation. In regions where HCl mixing ratios were essentially zero in the main run, HCl mixing ratios increase by up to 0.4 ppbv in this run. Figure 4 demonstrates that the model predicts $ClNO_2$ formation will almost completely deplete chloride concentrations in the locations where it occurs. The fact that $ClNO_2$ formation continues to occur throughout the night in the base case simulation is likely due to sea salt emissions, which act as a continual source of chloride.

Ground-level nitryl chloride mixing ratios increased significantly in this sensitivity analysis. On some days, the maximum ground-level nitryl chloride mixing ratio increased by more than a factor of three. The $ClNO_2$ mixing ratio in a single ground-level grid cell increased by up to 3200 pptv (more than a tenfold increase). In

addition, some decreases in $ClNO_2$ mixing ratios occurred in this sensitivity run. The maximum decrease was almost 300 pptv. These decreases may be caused by faster depletion of N_2O_5 when the $ClNO_2$ formation is not limited by chloride availability. Figure 5 shows the $ClNO_2$ mixing ratio in the base case heterogeneous chemistry run at 5am on September 1, 2006 as well as the changes in $ClNO_2$ mixing ratios that occurred in the simulation with no chloride limitations. The spatial distribution of the changes in $ClNO_2$ mixing ratios is similar to the distribution of depleted HCl mixing ratios shown in Figure 4. Also, the spatial extent of the $ClNO_2$ did not change significantly, only the magnitude of the mixing ratios. Table 2 summarizes the changes that occurred in ground level HCl and $ClNO_2$ mixing ratios in this simulation versus the base case simulation.

In addition to the ground-level mixing ratio, vertical profiles were also evaluated for this simulation. Figures 6 and 7 show the vertical profile of maximum and average $ClNO_2$ mixing ratios in the 4km domain at 1am for 4 nights. These figures show that on many nights $ClNO_2$ mixing ratios above 1000 m are virtually identical in the base case heterogeneous chemistry run and in the sensitivity run: August 31 (shown), September 1 (shown), September 2 (shown) , September 3 (not shown), September 5 (not shown), and September 9(not shown). On those nights, marine chloride availability appears to play no role in limiting $ClNO_2$ formation above 1000 m. Since most chloride is emitted at ground-level, it might be expected that chloride would be most concentrated at lower altitudes and that this would be a main limiting factor for $ClNO_2$ formation aloft. However, these results suggest that the opportunity for interaction between N_2O_5 and particle surfaces is the limiting factor for $ClNO_2$ formation aloft.

343 Based on this simulation, marine chloride availability greatly affected the
344 magnitude of $ClNO_2$ mixing ratios at ground-level (by up to a factor of 13), but not
345 aloft. In addition, horizontal spatial distributions were not affected within the marine
346 grid cells. The sensitivity run described in the next section tests the chloride
347 availability inland and gives insight into whether sufficient chloride is present over
348 terrestrial regions to lead to significant $ClNO_2$ formation.

349 ***3.2.1.2 Allowing $ClNO_2$ formation at inland locations***

350 In this sensitivity run, the "HCl switch" was used for the entire 4km and 12
351 km domains instead of just for the marine grid cells. $ClNO_2$ formation (Reaction 5)
352 proceeded wherever HCl mixing ratios were sufficiently high (above 0.5 pptv)
353 regardless of whether the location was marine or terrestrial. The reactive uptake and
354 yield used were the same as described above. When HCl dropped below 0.5 pptv,
355 Reaction (6) was used in the Houston Ship Channel grid cells and Reaction (7) was
356 used in all other cells. Previous modeling limited the geographic extent of $ClNO_2$
357 formation based on the assumption that it would only occur in a marine environment
358 where sea salt emissions are prevalent. This run eliminated that constraint, so that
359 $ClNO_2$ could form inland wherever HCl mixing ratios were high enough. There have
360 been no inland measurements of $ClNO_2$ in the Houston area, so model results cannot
361 be compared at this time with ambient data.

362 Figure 8 shows comparisons of $ClNO_2$ mixing ratios in the base case run and
363 in the sensitivity run which allowed formation at inland locations on the evening of
364 September 4, 2006. This figure shows that the model predicts sufficient
365 concentrations of chloride inland to form $ClNO_2$. In this sensitivity run, $ClNO_2$
366 mixing ratios were often above 400 pptv over the city of Houston. $ClNO_2$ mixing
367 ratios over land that was within 50 km of the shoreline were often as high as mixing

368 ratios over marine grid cells. On some days, $ClNO_2$ mixing ratios above 100 pptv
369 were predicted at locations more than 100 km inland.
370 Table 3 summarizes changes in domain-wide maximum ground-level $ClNO_2$
371 mixing ratios and domain-wide $ClNO_2$ mass at 5am. On some days the maximum
372 $ClNO_2$ mixing ratio was greater in the base case heterogeneous chemistry run and on
373 some days the maximum mixing ratios were greater in this sensitivity run. It appears
374 that when mixing ratios were greater in the base case heterogeneous chemistry run,
375 the maxima usually occurred where a NO_x plume first came in contact with marine
376 grid cells. In the sensitivity run where $ClNO_2$ formation could occur over land, the
377 N_2O_5 in the NO_x plume became partially depleted over land so the $ClNO_2$ mixing
378 ratios were lower but covered a greater area. In contrast, in the base case
379 heterogeneous chemistry run the NO_x plumes stayed relatively concentrated over land
380 and when these plumes suddenly contacted the marine environment, a great deal of
381 $ClNO_2$ was formed all at once, causing intense peaks over small areas. This was due
382 to the fact that the model predicted a lower reactive uptake coefficient over terrestrial
383 grid cells when no chloride was present (0.001) versus when sufficient chloride is
384 available to form $ClNO_2$ (0.03). This phenomenon can be seen in the Lake Charles,
385 LA plume in figure 8. The results reported here show that integrated $ClNO_2$ is larger
386 in the sensitivity run, even though $ClNO_2$ mixing ratios may be lower in marine
387 hotspots and that $ClNO_2$ formation becomes NO_x limited in the sensitivity run. On
388 days when the maximum $ClNO_2$ mixing ratio was greater in the sensitivity run, it
389 appears that the maximum occurred over land. This can be seen in Figure 8, which
390 shows $ClNO_2$ hotspots over Houston in the sensitivity run but not in the base case
391 heterogeneous chemistry run. The total $ClNO_2$ mass in the 4km domain was
392 significantly greater (between a factor of 3 and 22 greater depending on the day) when

393 $ClNO_2$ formation was allowed to occur over land. This indicates that $ClNO_2$
394 formation over land uses reservoirs of chloride that would not be accessed if $ClNO_2$
395 formation were restricted to marine cells and again supports the finding that integrated
396 $ClNO_2$ is larger when inland formation is included in the simulation.
397 Overall, this sensitivity run predicts that inland chloride concentrations are
398 indeed high enough to form $ClNO_2$. Inland formation is important for correctly
399 predicting the magnitude and extent of $ClNO_2$ mixing ratios. In addition, a great deal
400 more chloride mass will be converted to $ClNO_2$ when inland formation is taken into
401 account. Ambient measurements are still needed to verify these model results. It
402 should be noted again that these results represent an upper bound estimate for $ClNO_2$
403 formation since modeled yields were held constant at 75% but actual yields will
404 decrease as HCl concentrations drop.
405 **3.2.2. Sensitivity to changes in $ClNO_2$ yield**
406 The modeling performed above used a $ClNO_2$ yield in Reaction (5) of 75%.
407 As discussed previously, laboratory studies have shown that this yield depends on the
408 chloride concentration in the aerosol (Behnke et al., 1997; Schweitzer et al., 1998;
409 Roberts et al. 2009). Measurements and modeling results reported by Osthoff et al.
410 (2008), show that in the Gulf of Mexico this yield can range from 18% to 100%. Two
411 further modeling runs were performed (one with a 100% yield and one with an 18%
412 yield) to evaluate the upper and lower bounds of $ClNO_2$ yield for this region.
413 Table 4 shows the maximum ground-level mixing ratio changes in a single
414 grid cell for $ClNO_2$ in the low and high yield sensitivity runs. Changes are calculated
415 as the mixing ratio in the sensitivity run minus the mixing ratio in the base case run
416 and are evaluated over the entire 4km domain. As would be expected, there are large

417 decreases in $ClNO_2$ mixing ratios in the low yield run and large increases in $ClNO_2$
418 mixing ratios in the high yield run.

419 These sensitivity runs bound the uncertainty in the magnitude of mixing ratio
420 changes caused by the possibility of different yields. $ClNO_2$ mixing ratios could be
421 up to 85% lower or 70% higher if a different yield is used. These increase and
422 decreases are upper- and lower- bounds based on observed yields in the Gulf of
423 Mexico, but they show that the chemistry described in this work appears to be very
424 sensitive to $ClNO_2$ yield. It should also be noted that although the magnitude of
425 $ClNO_2$ mixing ratios changed with the yield, the spatial distribution of this compound
426 remained essentially unchanged.

427 **3.2.3 Explicit model representation of ClNO2 yield as a function of particulate**
428 **chloride concentration**

429 All of the uncertain parameters discussed above could be more explicitly
430 modeled by parameterizing the $ClNO_2$ yield as a function of particulate chloride
431 concentration. Studies by Roberts et al. (2009) and Behnke et al. (1997) have
432 reported $ClNO_2$ parameterizations based on laboratory data for Reactions (8) and (9).

433 $NO_2^+(aq) + H_2O(aq) \xrightarrow{k_8} HNO_3(g) + H^+(aq)$ Reaction (8)

434 $NO_2^+(aq) + Cl^-(aq) \xrightarrow{k_9} ClNO_2(g)$ Reaction (9)

435 Both Roberts et al. (2009) and Behnke et al. (1997) fitted their data to Equation (3),
436 reporting k_8/k_9 average values of 1/450 and 1/836 respectively.

437 $$y = \left\{ \left(\frac{k_8}{k_9} \right) \frac{[H_2O]}{[Cl^-]} + 1 \right\}^{-1}$$ Equation (3)

438 In Equation (3), y is $ClNO_2$ yield, (k_8/k_9) is the ratio of the rate constants for
439 Reactions (8) and (9), $[H_2O]$ is the molar density of water (mol/l), and $[Cl^-]$ is the
440 concentration of chloride in the aqueous phase (mol/l). Table 5 shows the particulate

441 chloride concentrations needed according to these two parameterizations to achieve
442 different $ClNO_2$ yields.
443 Roberts et al. (2009) reported that during the TexAQS II/GoMACCS field
444 campaign submicron aerosols measured on board the *Research Vessel Ronald H.*
445 *Brown* had a median chloride concentration of approximately 0.05 M and a maximum
446 chloride concentration of 1 M. Super-micron aerosols measured at the same time had
447 a median chloride concentration of approximately 2.5 M and a maximum
448 concentration of 10 M. This means that in the Gulf of Mexico, a $ClNO_2$ yield
449 between 29% and 40% would be expected on submicron aerosols and a yield between
450 95% and 97% would be expected on super-micron aerosols.
451 In order to add such a parameterization to a regional photochemical model it is
452 important that predictions of the particulate chloride concentrations be accurate. This
453 requires an accurate chlorine inventory, accurate partitioning between gas-phase HCl
454 and particulate-phase chloride (including acid displacement of Cl in sea salt aerosols),
455 and accurate determination of particulate water concentrations. Figures S7, S8, and
456 S9 (see supplemental information) show predicted nighttime gas-phase HCl mixing
457 ratios, $[Cl^-]$ in $PM_{2.5}$, and $[Cl^-]$ in coarse PM (PM with a diameter between 2.5 and 10
458 μm) from a CAMx model simulation which did not include any $ClNO_2$ chemistry, but
459 included the same emissions and meteorology of the model runs described above.
460 The HCl and particulate chloride concentrations shown in these figures should be
461 higher than would be predicted in a run that includes $ClNO_2$ chemistry since $ClNO_2$
462 formation depletes HCl/particulate chloride and cycles the chlorine into other forms.
463 Dibb (2009) and Osthoff et al. (2008) report that HCl measurements made during
464 TexAQS II in the Houston Ship Channel and at Moody Tower in downtown Houston
465 rarely dropped below 0.1 ppbv. HCl mixing ratios for those areas show in Figure S7

466 are generally less than this lower bound of 0.1 ppbv by a factor of two to ten. Since
467 partitioning between HCl and particulate chloride heavily favors the gas-phase state,
468 this indicates that total chloride is being under-predicted in the model. This is likely
469 due both to the large uncertainty in current anthropogenic chlorine emissions and the
470 fact that the sea salt inventory used in this modeling included open-ocean, but not
471 surf-zone emissions.

472 The [Cl^-] concentrations shown in Figures S8 and S9 can be compared to the
473 submicron and super-micron concentrations reported by Roberts et al. (2009),
474 although it should be noted that $PM_{2.5}$ concentrations will include some super-micron
475 particles and coarse PM will not contain all super-micron particles. The comparison
476 shows that on one night (August 30, 2006) [Cl^-] concentrations in fine PM are over-
477 predicted since the median concentration in marine regions is around 1 M and the
478 maximum concentration is above 10 M. The plot from September 5 shows [Cl^-] in the
479 range of that reported by Roberts et al. However the plots from September 2 and
480 September 8 show very low concentrations of [Cl^-], with median values less than 0.01
481 M. $ClNO_2$ formation on such particles would be negligible. The [Cl^-] concentration
482 in coarse PM is greater than the range reported by Roberts et al. (2009), with median
483 values above 10 M on several nights. The inaccuracy of model predictions for
484 particulate chloride concentrations may be a result of under-predicted chlorine
485 emissions, inaccurate gas/particle partitioning of HCl (specifically the movement of
486 chloride out of coarse aerosol through reactions with HNO_3), or inaccurate particulate
487 water content predictions.

488 The uncertainty in the model's ability to correctly predict particulate chloride
489 concentration in both coarse and fine PM means that explicitly representing $ClNO_2$
490 yield as a function of particulate chloride concentration in the current model could

lead either to significant under-predictions or significant over-predictions of $ClNO_2$ formation. Over-predictions of chloride at high concentrations (above 1 M) will not have a dramatic effect on the $ClNO_2$ formation rate since the yield at 1 M is already close to 100%. For example, at 2.5 M $ClNO_2$ yield from N_2O_5 uptake is above 95%. If the chloride concentrations were over-predicted by a factor of 10 (25 M), then the yield would be above 99% (only a 4% increase). Consequently over-predictions of coarse PM chloride concentrations are not a serious concern. In contrast, either an over-prediction or an under-prediction of $[Cl^-]$ in fine PM will significantly affect $ClNO_2$ formation rates. As mentioned above, at 0.05 M the expected yield is between 29% and 40%. A tenfold over-prediction in chloride concentration (0.5 M) would cause a yield of between 80% and 88%. A tenfold under-prediction in chloride concentration (0.005 M) would cause a yield of between 4% and 7%. Thus the $ClNO_2$ yield is particularly sensitive to chloride concentration in the range of values found in submicron aerosols.

3.3 The role of $ClNO_2$ in atmospheric chlorine cycling

In this model simulation, chlorine is emitted into the atmosphere in two forms: particulate chloride from sea salt emissions and Cl_2 from anthropogenic sources. The anthropogenic Cl_2 photolyzes to form chlorine radicals which proceed to participate in chemical reactions; HCl is a dominant product. This HCl can then partition into the particle-phase to form particulate chloride (the reverse phenomenon also occurs in which particulate chloride can partition to form gas-phase HCl). The particulate chloride and HCl reservoirs can be treated as one chloride reservoir since the model simulates that rapid equilibrium will be reached between gas and particle-phase chloride. Once chlorine is converted to HCl it can then react further to form $ClNO_2$, which in turn photolyzes to create chlorine radicals. As previously stated, the

chlorine radicals (whether from the photolysis of Cl_2 or $ClNO_2$) react to form HCl and other products. Because $ClNO_2$ acts both as a source and a sink for HCl, it forms a key step in chlorine cycling. Reactions (10), (11), and (12) show an example of how this chlorine cycling can occur leading to net Reaction (13).

$HCl + N_2O_5 \rightarrow ClNO_2 + HNO_3$ Reaction (10)

$ClNO_2 + h\nu \rightarrow NO_2 + Cl$ Reaction (11)

$CH_4 + Cl \rightarrow HCl + CH_3^{\cdot}$ Reaction (12)

$N_2O_5 + CH_4 \rightarrow NO_2 + HNO_3 + CH_3^{\cdot}$ Reaction (13)

N_2O_5 does not react directly with gas-phase HCl. Instead, reaction (10) is a representation of the net process that occurs when N_2O_5 reacts with particulate chloride and then HCl partitions into the particle form to replenish the loss of particulate chloride [essentially the same as Reaction (5)]. Reactions (10) – (12) provide a path by which chlorine may be continually cycled and reused in the atmosphere. It should also be noted that Reaction (12) is shown as one example of how Cl can be transformed into HCl; there are a variety of other Cl reactions in the CB IV chemical mechanism that also lead to the formation of HCl. However, without the inclusion of $ClNO_2$, there is no pathway in the chemical mechanisms used in current air quality models for non-reactive chloride (in the form of HCl or particulate chloride) to be quickly transformed back into reactive chlorine. The reaction of OH radicals with HCl to form a Cl radical and water has the potential to also cycle chlorine, but is not included in the CBIV chemical mechanism and was not considered here. In addition, it is important to note that Reaction (13) acts as a net radical source, while the OH + HCl reaction simply converts a HO_x radical into a chlorine radical.

539 To quantify the amount of $ClNO_2$ that results from the cycling described
540 above, two more simulations were performed. These simulations modeled $ClNO_2$ as a
541 chlorine sink. Photolysis was simulated using Reaction (14) instead of Reaction (11).
542 $ClNO_2 + h\nu \rightarrow NO_2$ Reaction (14)
543 One of the simulations used the N_2O_5 chemistry from the base simulation and the
544 other simulation used the N_2O_5 chemistry from the inland $ClNO_2$ formation sensitivity
545 run. Comparisons of total $ClNO_2$ mass present before dawn (at 5am) each morning in
546 the runs with chlorine cycling and in the new runs which do not cycle chlorine
547 through $ClNO_2$ are shown in Table 6. Decreases in total $ClNO_2$ mass from the base
548 case heterogeneous run to the simulation using Reaction (14) range from 28% to 56%.
549 Decreases in total $ClNO_2$ mass from the original inland $ClNO_2$ formation run to the
550 simulation using Reaction (14) range from 55% to 69%. The model simulations
551 predict that a large portion of the $ClNO_2$ in Southeast Texas has cycled through
552 $ClNO_2$ on previous nights.
553 This cycling is important because it means that greater amount of chlorine will
554 be in a form that is easily photolyzed into chlorine radicals which have an important
555 impact on urban ozone formation as discussed in Simon et al. (2008) and Chang and
556 Allen (2006a). Figures 9 and 10 show total photolyzable chlorine mass in the
557 simulations with and without cycling through $ClNO_2$ in the base case and inland
558 formation simulations respectively. In these simulations the majority of photolyzable
559 chlorine is in the form of Cl_2 and $ClNO_2$. Daily photolyzable chlorine mass in Figures
560 9 and 10 was calculated as total 24 hr emissions of Cl_2 plus total $ClNO_2$ mass present
561 just before sunrise. These figures show that when cycling through $ClNO_2$ is shut off,
562 the total reactive chlorine mass in the atmosphere decreases significantly. On some
563 days over two thirds of the reactive chlorine mass present in the atmosphere has been

564 cycled through $ClNO_2$. Properly modeling this process will be important for properly
565 simulating chlorine chemistry in regional photochemical models.

566 One additional factor must be considered when evaluating the impact of
567 $ClNO_2$ formation on chlorine cycling: deposition. HCl from the cycling pathway
568 described above is mostly formed in the first few hours after sunrise when $ClNO_2$
569 photolyzes. For $ClNO_2$ to play a major role in chlorine cycling, this HCl must remain
570 in the atmosphere through the day (at least 12 hours) since the $ClNO_2$ formation
571 process occurs predominately at night. If the deposition lifetime of HCl were short (on
572 the order of several hours), then the majority of HCl formed through Reaction (12)
573 and similar reactions would be lost before it could react with N_2O_5 to form $ClNO_2$.
574 CAMx models dry deposition based on the methods developed by Wesely (1989)
575 which account for Henry's law, diffusion, reactivity, and surface resistance. An
576 average deposition lifetime for the entire 4km modeling domain (including the
577 boundary layer and the free troposphere) was calculated as the total mass of HCl
578 (moles) divided by the deposition rate of HCl (moles/day). During the modeling
579 simulation this value was 16.8 days. The lifetime with respect to deposition within
580 the boundary layer is considerably shorter and was calculated as the average dry
581 deposition velocity (m/s) divided by the boundary layer height (m). The deposition
582 lifetime for HCl during the simulation in the boundary layer was 3.1 days in marine
583 areas and 0.74 days (17.8 hours) in terrestrial areas. These deposition lifetimes for
584 HCl are in the same range as the global deposition lifetime reported by Graedel and
585 Keene (1995) for HCl: 1.44 days in the boundary layer and 73 days in the free
586 troposphere. Even with the relatively short deposition lifetime of HCl in the boundary
587 layer, reactions of particulate chloride with N_2O_5 lead to significant chlorine cycling.

588 This process appears to compete effectively with deposition as a major
589 loss/transformation process for HCl and particulate chloride.
590 Previous modeling studies have looked at other chlorine cycling pathways in
591 the atmosphere. Notably, the reaction of OH radicals with HCl to form a Cl radical
592 and water has the potential to also cycle chlorine (Pechtl and von Glasow, 2007).
593 However, that reaction cycles a smaller amount of Cl than the heterogeneous N_2O_5
594 reaction pathway under the heavily polluted conditions encountered in this study.
595 With a rate constant of 8×10^{-13} cm^3/molecule-sec, the reaction rate in heavily
596 polluted conditions (HCl concentration of 1 ppbv and OH concentration of 0.5 pptv)
597 is approximately 30 pptv/hr during the day and much less at night when OH
598 concentrations are small. Over the period of 12 hours of sunlight, the HCl + OH
599 reaction could create approximately 360 pptv of Cl with no dilution, much less than
600 $ClNO_2$ concentrations measured by Osthoff et al (2008). Other chlorine cycling
601 pathways (reactions of OH, $ClONO_2$, and NO_3 on sea salt aerosols to produce Cl_2)
602 have been modeled by Knipping and Dabdub (2003). They reported that the
603 chemistry only led to maximum Cl_2 concentrations of 12 pptv in the late evening and
604 pre-dawn. The $ClNO_2$ concentrations measured by Osthoff et al (2008) were two
605 orders of magnitude greater than the Cl_2 concentrations from the Knipping and
606 Dabdub modeling. Although these previous studies show that other chlorine cycling
607 pathways may exist in the atmosphere, the ambient measurements made by Osthoff et
608 al (2008) are direct evidence that the $ClNO_2$ pathway is an important chlorine cycling
609 mechanism in a major urban area

610 **4. Conclusions**

611 The work reported here examined the effect of chloride limitation on $ClNO_2$
612 formation using a regional photochemical model. Modeling predicted peak $ClNO_2$

613 concentrations of above 1 ppbv based on parameters specific to Southeast Texas,
614 which were in line with measurements made in this region. These concentrations may
615 not be applicable to other regions.

616 This work identified key uncertainties in the modeling of heterogeneous N_2O_5
617 chemistry including yield of $ClNO_2$ and the availability of chloride at inland
618 locations. Eliminating the dependence of $ClNO_2$ formation on chloride availability
619 caused increases in $ClNO_2$ mixing ratios of up to a factor of 13. This suggests that
620 chloride availability is a major limiting factor in this process at ground level. The
621 sensitivity run which allowed $ClNO_2$ formation to occur at terrestrial locations
622 predicted that chloride mixing ratios are high enough inland to cause significant
623 $ClNO_2$ formation over the entire Houston area. Sensitivity runs showed that the
624 modeled $ClNO_2$ concentration is very sensitive to yield. Although this parameter is
625 highly uncertain, the yields used in this study are as accurate as any other in the
626 absence of realistic model simulation for aerosol chloride molarity. Further work is
627 suggested to increase model accuracy in predicting particulate chloride concentrations
628 so that yield can be more accurately simulated in the future. In addition, there are two
629 major areas for which field studies are needed to better understand the chemistry
630 investigated in this work. First, no measurements of $ClNO_2$ have been made at inland
631 locations. Further field work is suggested to verify the model prediction that
632 significant $ClNO_2$ mixing ratios may occur over land. Second, more ambient
633 measurements are needed to determine if parameterization of $ClNO_2$ yield based on
634 laboratory data hold in the ambient atmosphere.

635 Finally, this work not only evaluated the effect of chloride availability on
636 $ClNO_2$ formation, but also investigated how this formation process may affect
637 chlorine cycling in the atmosphere. Modeling analyses suggest that chemical cycling

of chlorine through HCl and $ClNO_2$ is important and that on many nights the majority of photolyzable chlorine present in the atmosphere goes through chloride/active chlorine cycling. Although modeling techniques here predict an upper-bound for the effect of $ClNO_2$ chemistry, this work shows that $ClNO_2$ plays an important role in chlorine cycling. Current photochemical air quality modeling programs do not include this cycling pathway for chlorine, so once Cl radicals react to form HCl there is no efficient pathway to convert the chloride back into reactive species. Other pathways not included in this modeling could also lead to chlorine cycling in the atmosphere (although to a lesser degree under conditions relevant to southeast Texas) and should be included in future modeling studies. The work described here has shown that in order to properly model atmospheric chlorine chemistry and its effects on urban air pollution in Southeast Texas, it will be essential to include this $ClNO_2$ formation pathway and chlorine cycling mechanism. Although this work used modeling parameterized specific to Southeast Texas, the general mechanism in which Cl cycles between HCl during the day and $ClNO_2$ at night may be more widely applicable and should be investigated more fully through modeling and measurement studies in other regions.

Acknowledgements

Support for this work was provided by the Texas Air Research Center.

Disclaimer

The United States Environmental Protection Agency through its Office of Research and Development collaborated in the research described here. It has been subjected to Agency review and approved for publication.

References

Aldener, M., Brown, S.S., Stark, H., Williams, E.J., Lerner, B.M., Kuster, W.C., Goldan, P.D., Quinn, P.K., Bates, T.S., and Fehsenfeld, F.C., 2006. Reactivity

and loss mechanisms of NO_3 and N_2O_5 in a marine environment: results from in-situ measurements during NEAQS 2002., J. Geophys. Res., 111, D23S73, doi:10.1029/2006JD007252.

Behnke, W., George, C., Scheer, V., Zetzsch, C., 1997. Production and decay of $ClNO_2$, from the reaction of gaseous N_2O_5 with NaCl solution: bulk and aerosol experiments. Journal of Geophysical Research-Atmospheres 102 (D3), 3795-3804.

Brown, S., Ryerson, T., Wollny, A., Brock, C., Peltier, R., Sullivan, A., Weber, R., Dube, W., Trainer, M., Maegher, J., Fehsenfeld, F., Ravishankara, A, 2006. Variability in nocturnal nitrogen oxide processing and its role in regional air quality. Science 311, 67-70.

Brown, S., Dube, W. P., Fuchs, H., Ryerson, T. B., Wollny, A.G., Brock, C.A., Bahreini, R., Middlebrook, A. M., Neuman, J.A., Atlas, E., Roberts, J.M., Osthoff, H.D., Trainer, M., Fehsenfeld, F.C., Ravishankara, A.R., 2009 Reactive uptake coefficients for N_2O_5 determined from aircraft measurements during the second Texas Air Quality Study: comparison to current model parameterizations. Journal of Geophysical Research 114, D00F10, doi 10.1028/2008JD011679.

Chang, S., Allen, D.T., 2006a. Atmospheric chlorine chemistry in southeast Texas: Impacts on ozone formation and control. Environmental Science and Technology *40,* 251-262.

Chang, S., Allen, D.T., 2006b, Chlorine chemistry in urban atmospheres: Aerosol formation associated with anthropogenic chlorine emissions in southeast Texas. Atmospheric Environment 40 (S2), S512-S523.

Davis, J.M., Bhave, P.V., Foley, K.M., 2008, Parameterization of N_2O_5 reaction probabilities on the surface of particles containing ammonium sulfate and nitrate. Atmospheric Chemistry and Physics 8, 5295-5311.

Jack Dibb, Research Associate Professor, Climate Change Research Center, University of New Hampshire, Durham, NH. Personal Communication, February 2009.

ENVIRON International Corporation, 2008. User's Guide to the Comprehensive Air quality Model with Extensions, version 4. Accessed at http://www.camx.com.

U.S. Environmental Protection Agency (EPA), 2006. Emissions Modeling Clearinghouse Shapefiles to use with the Spatial Surrogate Tool. Accessed in December 2006 at: http://www.epa.gov/ttn/chief/emch/spatial/spatialsurrogate.html

U.S. Environmental Protection Agency (EPA), 2008. Technology Transfer Network Clearinghouse for Inventories & Emissions Factors, Criteria Pollutant Emissions Summary Files. See: http://www.epa.gov/ttn/chief/net/critsummary.html

Evans, M.J. and Jacob, D.R., 2005. Impact of new laboratory studies of N_2O_5 hydrolysis on global model budgets of tropospheric nitrogen oxides, ozone, and OH. Geophys. Res. Let 32, L09813, doi:10.1029/2005GL022469.

Finlayson-Pitts, B.J., Ezell, M.J., Pitts, J.N. Jr, 1989. Formation of chemically active chlorine compounds by reactions of atmospheric NaCl particles with gaseous N_2O_5 and $ClONO_2$. Nature 337, 241-244.

Gery, M.W., Whitten, G.Z., Killus, J.P., and Dodge, M.C., 1989. A photochemical kinetics mechanism for urban and regional scale computer modeling. Journal of Geophysical Research 94, 925-956.

713 Graedel, T.E., Keene, W.C., 1995. Tropospheric budget of reactive chlorine. Global
714 Biogeochemical Cycles 9(1), 47-77.
715 Knipping, E. M., Dabdub, D., 2003. Impact of chlorine emissions from sea-salt
716 aerosol on coastal urban ozone. Environmental Science and Technology 37,
717 275-284.
718 MIMS User's Guide. Accessed in December 2006 at:
719 http://www.ie.unc.edu/cempd/projects/mims/spatial/srgtool/
720 Morris, R.J., Koo, B., Yarwood, G., 2005. Evaluation of multisectional and two-
721 sectional particulate matter photochemical grid models in the western United
722 States. Journal of the Air and Waste Management Association 55, 1683-1693.
723 Nenes, A., Pandis, S.N., Pilinis, C., 1998. ISORROPIA: a new thermodynamic
724 equilibrium model for multiphase multicomponent inorganic aerosols.
725 Aquatic Geochemistry 4(1), 123-152.
726 Ngan, F., 2008). Classification of weather patterns and improvement of
727 meteorological inputs for TexAQS-II air quality simulations, Ph.D.
728 Dissertation, University of Houston.
729 Osthoff, H. D., Roberts, J.M., Ravishankara, A.R., Williams, E. J., Lerner, B.M.,
730 Sommariva, R., Bates, T.S., Coffman, D., Quinn, P.K., Dibb, J.E., Stark, H.,
731 Burkholder, J.B., Talukdar, R.K., Maegher, J., Fehsenfeld, F.C., Brown, S.S.,
732 2008. High levels of nitryl chloride in the polluted subtropical marine
733 boundary layer. Nature Geosciences 1(5), 323-328.
734 Pandis, S.N., Wexler, A.S., Seinfeld, J.H., 1993. Secondary organic aerosol
735 formation and transport II, predicting the ambient secondary organic aerosol
736 size distribution. Atmospheric Environment 27A, 2403-2416.
737 Pechtl, S., von Glasow, R., 2007. Reactive chlorine in the marine boundary layer in
738 the outflow of polluted continental air: a model study. Geophysical Research
739 Letters 34, L11813.
740 Roberts, J.M., Osthoff, H.D., Brown, S.S., Ravishankara, A.R., Coffman, D., Quinn,
741 P., Bates, T., 2009. Laboratory Studies of Products of N2O5 Uptake on Cl-
742 Containing Substrates, Geophys. Res. Lett., 2009GL039727, submitted.
743 Santarpia, J. L., R. Li, D. R. Collins, 2004. Direct measurement of the hydration state
744 of ambient aerosol populations. Journal of Geohpysical Research –
745 Atmospheres 109 D18209, doi:10.1029/2004JD004653.
746 Schweitzer, F., Mirabel, P., George, C., 1998. Multiphase chemistry of N_2O_5, $ClNO_2$,
747 and $BrNO_2$. Journal of Physical Chemistry 102, 3942-3952.
748 Simon, H., 2008. Heterogeneous N_2O_5 chemistry in the Houston atmosphere, Ph.D.
749 Dissertation, University of Texas at Austin. Available through the UT
750 Libraries at:
751 http://www.lib.utexas.edu/etd/d/2008/simonh18695/simonh18695.pdf#page=3
752 Simon, H., Allen, D.T., Wittig, A.E., 2008. Fine particulate matter emissions
753 inventories: Comparison's of emissions estimates with observations from
754 recent field programs. Journal of the Air and Waste Management Association
755 58(2), 320-343.
756 Simon, H, Kimura, Y., McGaughey, G., Allen, D.T., Brown, S.S., Osthoff, H.D.,
757 Roberts, J.M., Byun, D., Lee, D., 2009. Modeling the Impact of $ClNO_2$ on
758 Ozone Formation in the Houston Area. Journal of Geophysical Research 114,
759 D00F03, doi:10.1029/2008JD010732.
760 Tanaka, P.L, Allen, D.T., McDonald-Buller, E.C., Chang, S., Kimura, Y., Mullins,
761 C.B., Yarwood, G., Neece, J.D., 2003. Development of a chlorine mechanism

for use in the carbon bond IV chemistry model. Journal of Geohpysical Research - Atmospheres 108(D4), 4145.

Tesche, T.W., Morris, R., Tonnesen, G., McNally, D., Boylan, J., Brewer, P., 2006. CMAQ/CAMx annual 2002 performance evaluation of the eastern US. Atmospheric Environment 40, 4906-4919.

Thornton, J. A., Abbatt, J. P. D., 2005. N_2O_5 reaction on submicron sea salt aerosol: Kinetics, products, and the effect of surface active organics. Journal of Physical Chemistry 109, 10004-10012.

Wang, L., Thompson, T., McDonald-Buller, E.C., Webb, A., Allen, D.T., 2007. Photochemical modeling of emissions trading of highly reactive volatile organic compounds in Houston, Texas. 2. Incorporation of chlorine emissions. Environmental Science and Technology 41, 2103-2107.

Wesely, M.L., 1989. Parameterization of Surface Resistances to Gaseous Dry Deposition in Regional-Scale Numeric Models. Atmospheric Environment 23, 1293-1304.

Yarwood, G. Whitten, G.Z., Rao, S., 2005. Updates to the carbon bond 4 photochemical mechanism, prepared for the Lake Michigan Air Directors Consortium, Des Plaines, IL. Available at: http://www.ladco.org/reports/rpo/modeling/camx_cb4.pdf.

Tables

Table 1: Average and Maximum ground-level concentrations for N_2O_5, $ClNO_2$, and HNO_3 for nights in the modeled episode in the 4km domain.

	N_2O_5 (pptv)		$ClNO_2$ (pptv)		HNO_3 (pptv)	
Night of:	**Average**	**Maximum**	**Average[a]**	**Maximum**	**Average**	**Maximum**
Aug 30-Aug 31	78	3885	14	419	719	3338
Aug 31-Sep1	280	8526	85	1034	1519	6297
Sep 1- Sep2	304	8016	81	1210	1830	9675
Sep 2 - Sep 3	189	8906	37	362	1000	6286
Sep 3 - Sep 4	191	7362	51	256	1039	6113
Sep 4 - Sep 5	92	4565	31	400	677	4415
Sep 5 - Sep 6	18	2235	17	276	459	1946
Sep 6 - Sep 7	199	6215	101	1002	937	7260
Sep 7 - Sep 8	316	8165	97	911	1995	16 025
Sep 8 - Sep 9	333	13 547	161	882	2620	13 964

a) Average values for $ClNO_2$ were only calculated for marine grid cells

Table 2: Summary of changes in $ClNO_2$ and HCl concentrations when excess chloride is present.

Night of:	**Max $ClNO_2$ conc in main run (pptv)**	**Max $ClNO_2$ conc with excess chloride (pptv)**	**Max $ClNO_2$ increase in a single grid cell[a] (pptv)**	**Max $ClNO_2$ increase in a single grid cell[b] (%)**	**Max change in HCl in a single grid cell[c] (ppbv)**
Aug 30 – 31	419	928	630	210	0.2
Aug 31 - Sep 1	1034	2606	2020	670	0.1
Sep 1-2	1210	3733	3244	1110	0.3
Sep 2-3	362	800	500	220	0.1
Sep 3-4	256	817	615	470	0.4
Sep 4-5	400	996	616	200	0.1
Sep 5-6	276	397	242	280	0.2
Sep 6-7	1002	1716	1115	610	0.2

Sep 7-8	911	2535	2216	1270	0.3
Sep 8-9	882	1343	901	390	0.4

a) Change in $ClNO_2$ concentration calculated as concentration in sensitivity run simulation (excess chloride) minus concentration in base case run

b) Percent increases only calculated for grid cells in which the $ClNO_2$ concentration was greater than 50 pptv in the sensitivity run simulation

c) Calculations done between the hours of 8pm and 5am

Table 3: Comparison of $ClNO_2$ concentration and mass in base case run and sensitivity run which allows inland $ClNO_2$ formation.

Night of:	Maximum $ClNO_2$ concentration in the base case run (pptv)	Maximum $ClNO_2$ concentration in sensitivity run (pptv)	$ClNO_2$ mass in the 4km domain in base case run at 5am (metric tons)	$ClNO_2$ mass in the 4km domain in sensitivity run at 5am (metric tons)
Aug 30 - 31	419	539	4.8	103.8
Aug 31 - Sep 1	1034	630	9.7	113.6
Sep 1-2	1210	800	15.7	97.4
Sep 2-3	362	241	16.5	88.6
Sep 3-4	256	682	14.7	80.9
Sep 4-5	400	494	10.7	97.4
Sep 5-6	276	220	11.3	156.4
Sep 6-7	1002	1010	29.6	125.2
Sep 7-8	911	909	51.7	165.8
Sep 8-9	882	2051	52.2	197.5

Table 4: Changes in ground-level $ClNO_2$ concentrations in the low and high $ClNO_2$ yield sensitivity runs in the 4km domain. All changes in ClNO2 concentrations are defined as (conc in sensitivity run) - (conc in base case run).

Night of:	$ClNO_2$ Yield = 0.18		$ClNO_2$ Yield = 1.00	
	Max decrease in $ClNO_2$ (pptv)	max decrease in $ClNO_2$ (%)	max increase in $ClNO_2$ (pptv)	Max increase in $ClNO_2$ (%)
Aug 30-31	-332	-86	137	68
Aug 31-Sep 1	-706	-85	289	67
Sep 1-2	-896	-85	373	60
Sep 2-3	-273	-79	122	63
Sep 3-4	-200	-78	85	45
Sep 4-5	-322	-81	137	61
Sep 5-6	-194	-76	72	54
Sep 6-7	-808	-83	355	65
Sep 7-8	-579	-80	232	57
Sep 8-9	-654	-80	285	44

Table 5: $ClNO_2$ yield parameterized by $[Cl^-]$ using k_8/k_9 values reported by Behnke et al. (1997) and Roberts et al. (2009)

$ClNO_2$ yield (%)	Required $[Cl^-]$ (M) from Roberts et al. (2009)	Required $[Cl^-]$ (M) from Behnke et al. (1997)
1	0.001	0.001
10	0.014	0.007
50	0.123	0.066
75	0.370	0.199
90	1.111	0.598

Table 6: Decreases in $ClNO_2$ mass at 5am in the 4km domain resulting from turning off chlorine cycling through $ClNO_2$

Date	Base case run			Inland Cl run		
	$ClNO_2$ mass: Cl cycling (metric tons)	$ClNO_2$ mass: no Cl cycling (metric tons)	Decrease in $ClNO_2$ mass (%)	$ClNO_2$ mass: Cl cycling (metric tons)	$ClNO_2$ mass: no Cl cycling (metric tons)	Decrease in $ClNO_2$ mass (%)
31-Aug	4.8	2.7	44	103.8	36.5	65
1-Sep	9.7	7.0	28	113.6	46.9	59
2-Sep	15.7	11.4	28	97.4	43.8	55
3-Sep	16.5	9.8	40	88.6	35.2	60
4-Sep	14.7	10.6	28	80.9	32.4	60
5-Sep	10.7	4.9	55	97.4	30.4	69
6-Sep	11.3	4.9	56	156.4	53.9	66
7-Sep	29.6	19.8	33	125.2	54.5	57
8-Sep	51.7	31.3	39	165.8	64.8	61
9-Sep	52.3	35.2	33	197.5	84.0	58

808

809

810

811

812

813

814 **Figures**

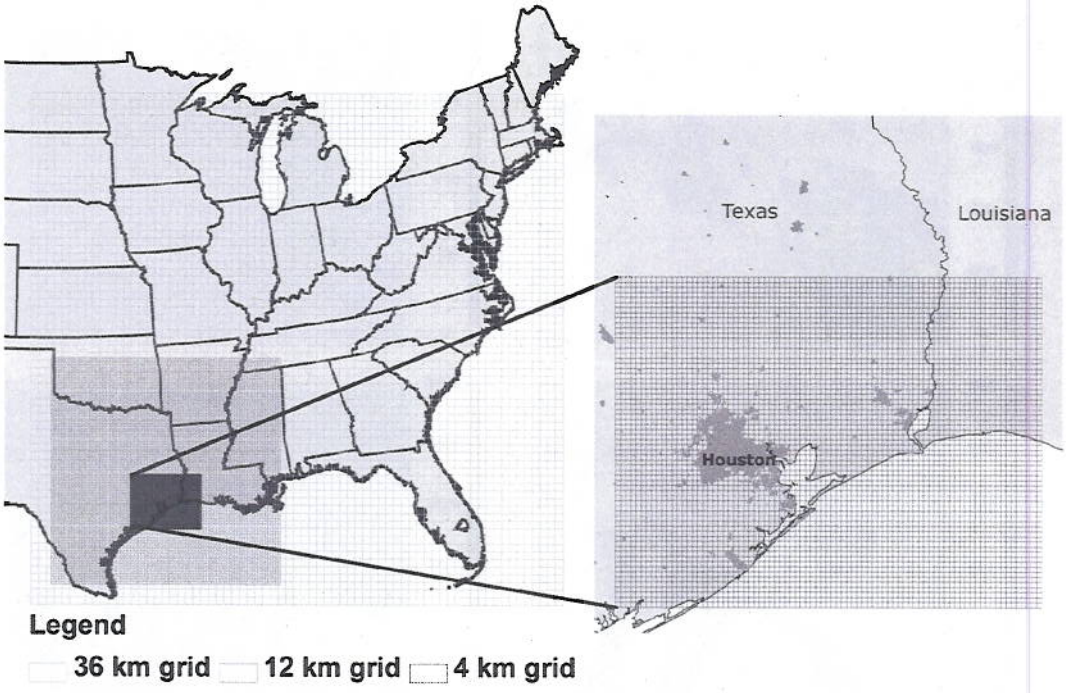

815

816 Figure 1: Nested domains used in CAMx modeling

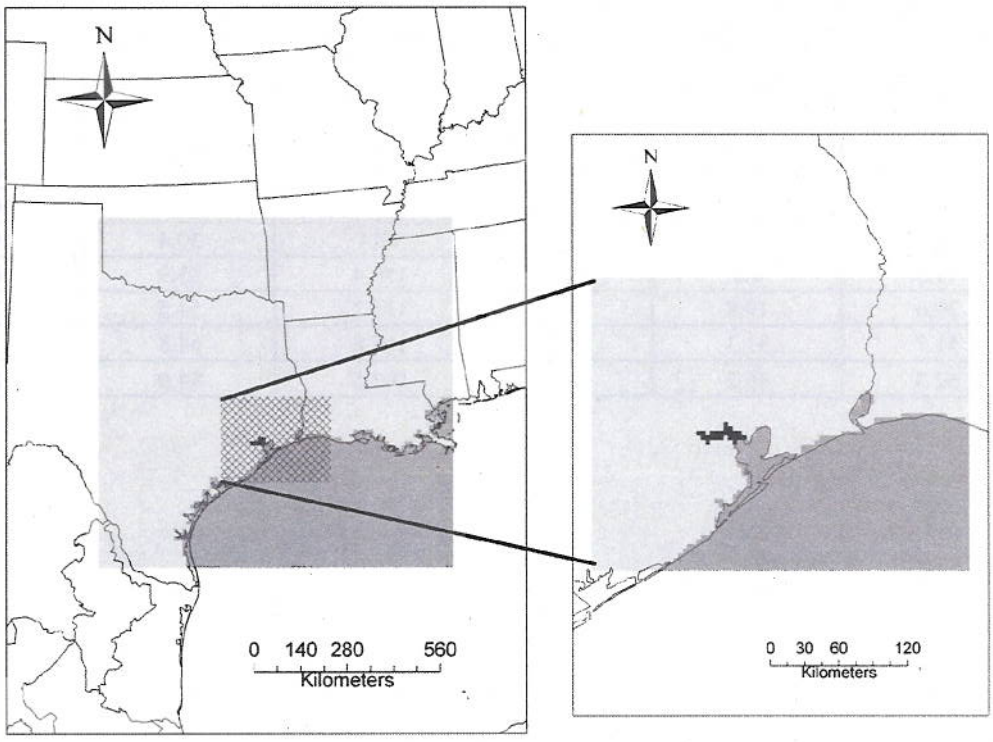

Figure 2: Regions used to define heterogeneous N_2O_5 reaction rate parameters. Region 1 is shown in dark gray, region 2 is shown in black, and region 3 is shown in light gray.

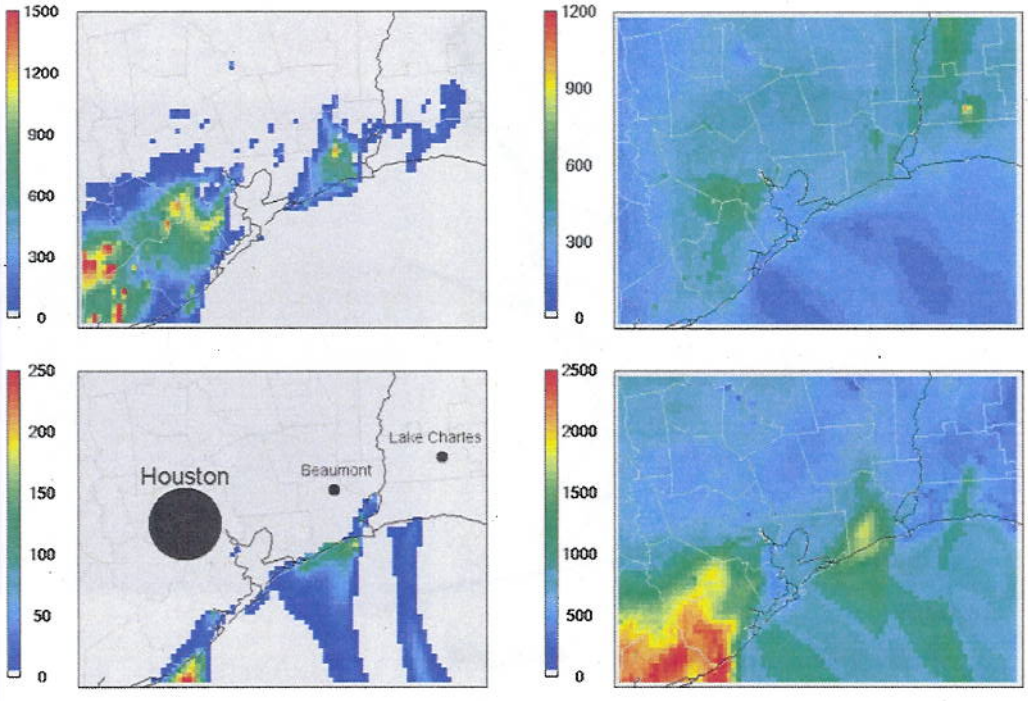

825 Figure 3: Pollutant concentrations at 4am on Aug 31, 2006: N_2O_5 (pptv) at upper left,
826 aerosol surface area (μm2/cm3) at upper right, $ClNO_2$ (pptv) at lower left, HNO_3
827 (pptv) at lower right.
828

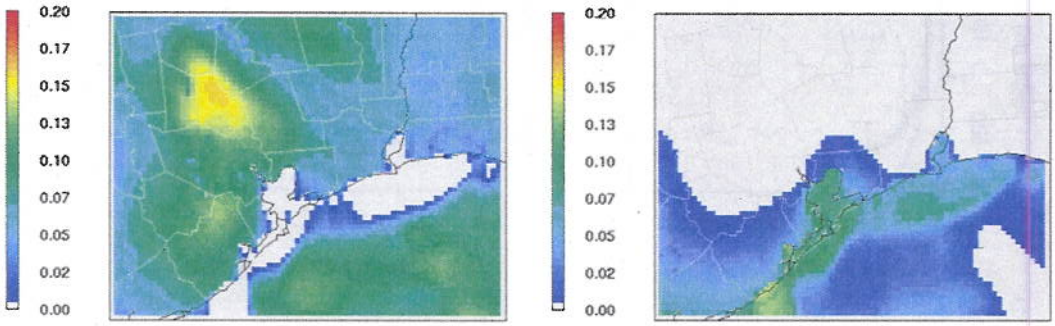

829
830 Figure 4: HCl mixing ratio (ppbv) in base case run on September 1, 2006 at 5am
831 (left). Change in HCl mixing ratio (ppbv) caused by not depleting HCl when ClNO2
832 is formed on September 1, 2006 at 5am (right).
833

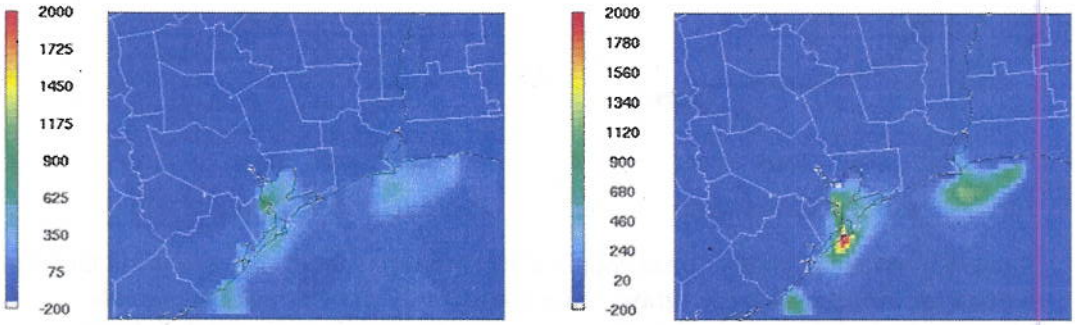

834
835 Figure 5: ClNO2 mixing ratio (pptv) in base case run on September 1, 2006 at 5am
836 (left). Change in ClNO2 mixing ratio (pptv) when excess chloride is present on
837 September 1, 2006 at 5 a.m. (right).

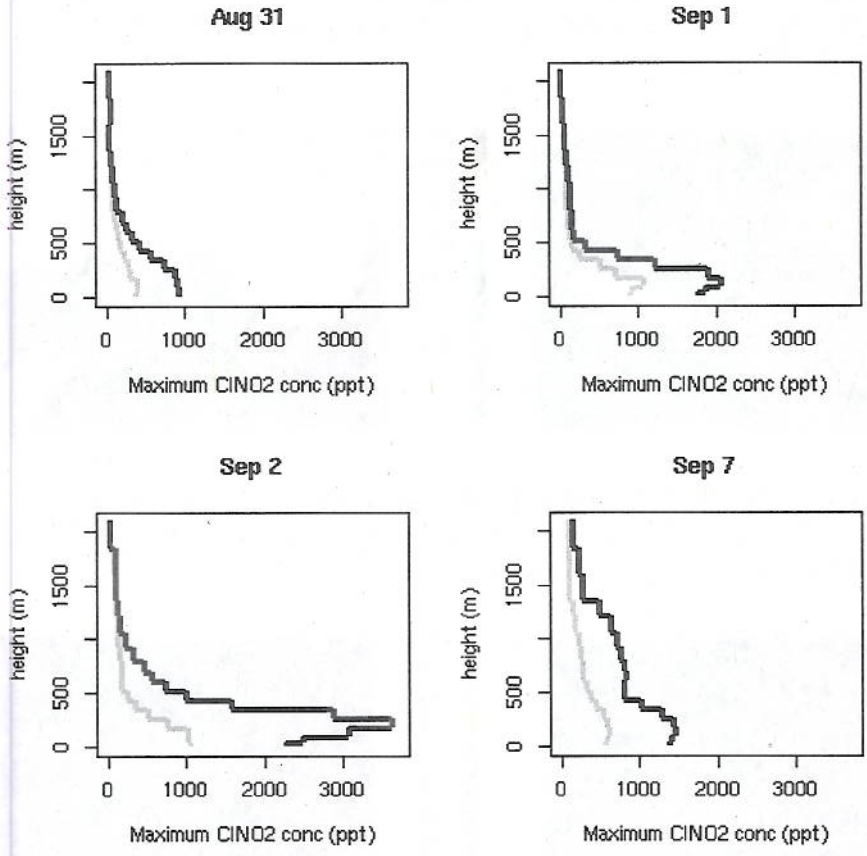

838
839 Figure 6: Vertical profiles of maximum $ClNO_2$ mixing ratios (pptv) at 1am in the 4km
840 domain for the base case run (gray) and the sensitivity run with excess chloride
841 (black). Maximum is reported as the maximum concentration at each height (this
842 value may occur in different grid cells in different vertical layers)

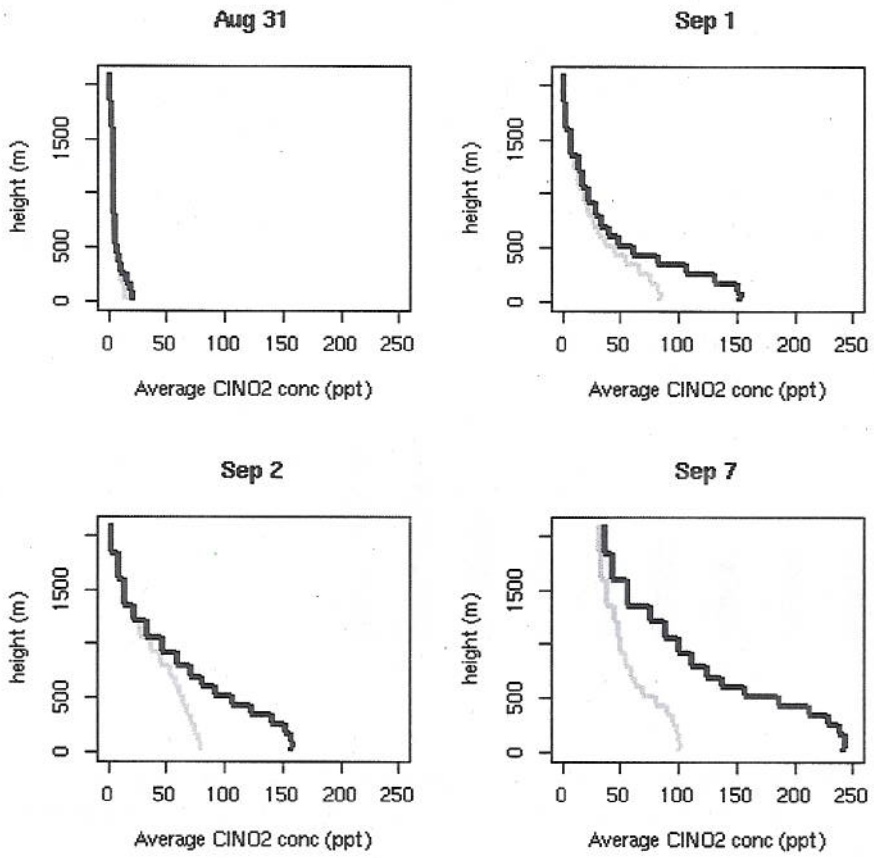

Figure 7: Vertical profiles of average $ClNO_2$ mixing ratios (pptv) at 1am in the 4km domain for the base case run (gray) and the sensitivity run with excess chloride (black).

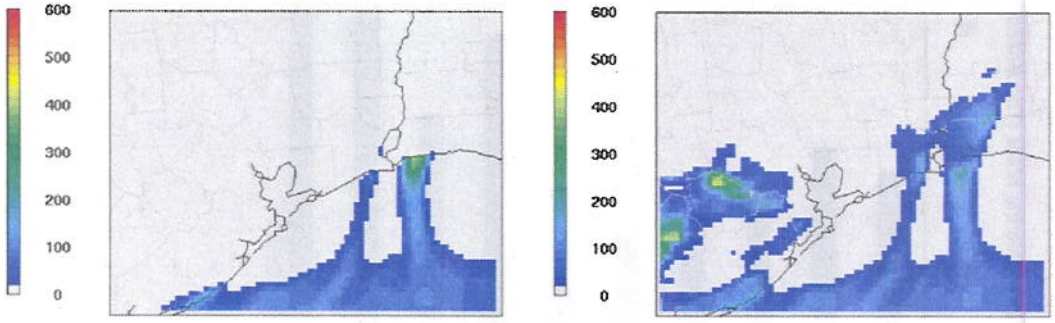

Figure 8: Modeled $ClNO_2$ mixing ratios (pptv) on September 4, 2006 at 8pm in the base case run (left) and in the sensitivity run which allowed inland $ClNO_2$ formation (right).

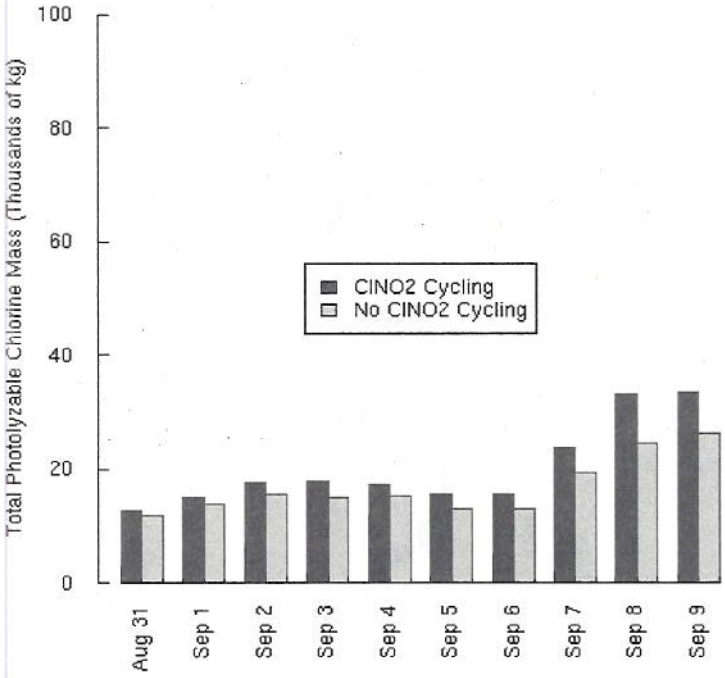

853
854 Figure 9: Total daily photolyzable chlorine mass present (Cl_2 and $ClNO_2$) with and
855 without cycling through $ClNO_2$ for simulations that only allowed $ClNO_2$ formation in
856 marine grid cells.

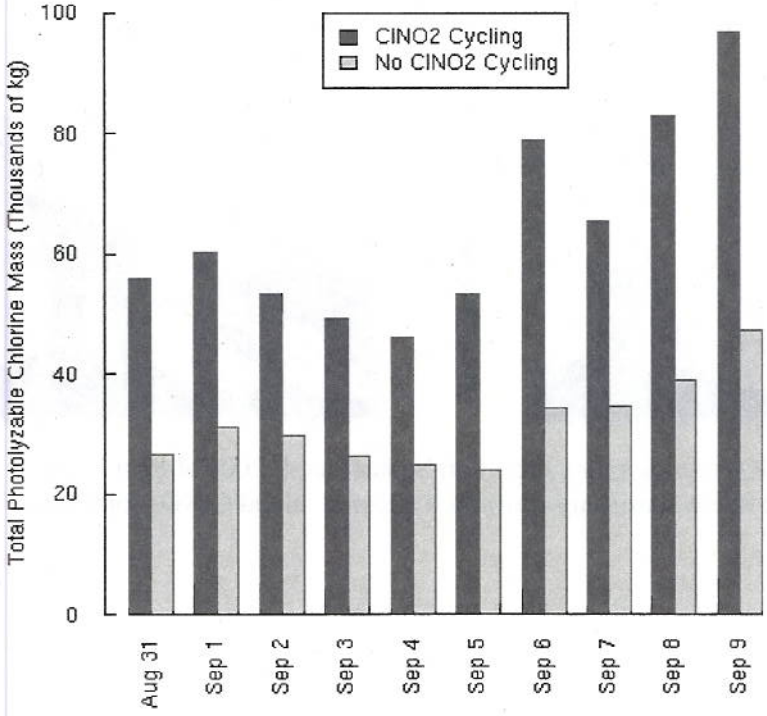

857

858 Figure 10: Total daily photolyzable chlorine mass present (Cl_2 and $ClNO_2$) with and
859 without cycling through $ClNO_2$ for simulations that allowed $ClNO_2$ formation both at
860 marine and inland locations.
861
862